

Dual channel selective fluorescent detection of Al³⁺ and PPi in mixed aqueous media: DFT studies and cell imaging applications.

Rabiul Alam^a, Tarun Mistri^a, Rahul Bhowmick^a, Atul Katarkar^b, Keya Chaudhuri^b and
Mahammad Ali^{a*}

^aDepartment of Chemistry Jadavpur University, Kolkata 700 032, India; Fax: 91-33-2414-6223, E-mail: mali@chemistry.jdvu.ac.in

^bMolecular & Human Genetics Division , CSIR-Indian Institute of Chemical Biology , 4 Raja S.C. Mullick Road, Kolkata-700032, India

Supporting Information for Publication

Table of contents

1. ¹H NMR spectrum of DFC-EN-*p*-Ph-NO₂in DMSO-d₆, in Bruker 300 MHz instrument.

Fig. S1

2. ¹³C NMR spectrum of DFC-EN-*p*-Ph-NO₂in DMSO-d₆, in Bruker 300 MHz instrument

Fig. S2

3. Mass spectrum of DFC-EN-*p*-Ph-NO₂

Fig. S3

4. Mass spectrum of Al complex

Fig.S3a

5. FT-IR spectrum of DFC-EN-*p*-Ph-NO₂ in MeOH

Fig. S4

6. Job's plot DFC-EN-*p*-Ph-NO₂ + Al³⁺

Fig.S5

7. LOD determination.

Fig. S6

8. Overall Spectra upon the addition of PPi on the Al³⁺ complex and in excess.

Fig. S7

9. Overall Spectra upon the addition of Al³⁺ on the PPi complex.

Fig.S8

10. Solvent dependence study of absorbance and emission spectra of
DFC-EN-*p*-Ph-NO₂, DFC-EN-*p*-Ph-NO₂+Al³⁺ and DFC-EN-*p*-Ph-NO₂+PPi complex.

Fig.S9

11. ¹H-NMR chemical shifts in ppm of selected H-atoms in DMSO-d₆

Table S1

12. Selective bond distance and bond angles of DFC-EN-*p*-Ph-NO₂ + Al³⁺ complex **Table S2a**

13. Selective bond distance and bond angles of DFC-EN-*p*-Ph-NO₂. **Table S2b**

14. Selective bond distance and bond angles of DFC-EN-*p*-Ph-NO₂ + PPi complex. **Table S3**

15. DFT optimized geometry of ligandas well as complexes with Al³⁺ and PPi
Fig.S10

**16. HOMO-LUMO energy separation in ligand DFC-EN-*p*-Ph-NO₂ as well as complexes
with Pi, ATP and PPi.**

Fig.S11.

The comparable calculated optical transitions with Experimental UV/Vis values for the ligand
(DFC-EN-*p*-Ph-NO₂) and complex (3)

Table S4

17. MTT assay
Fig. S12

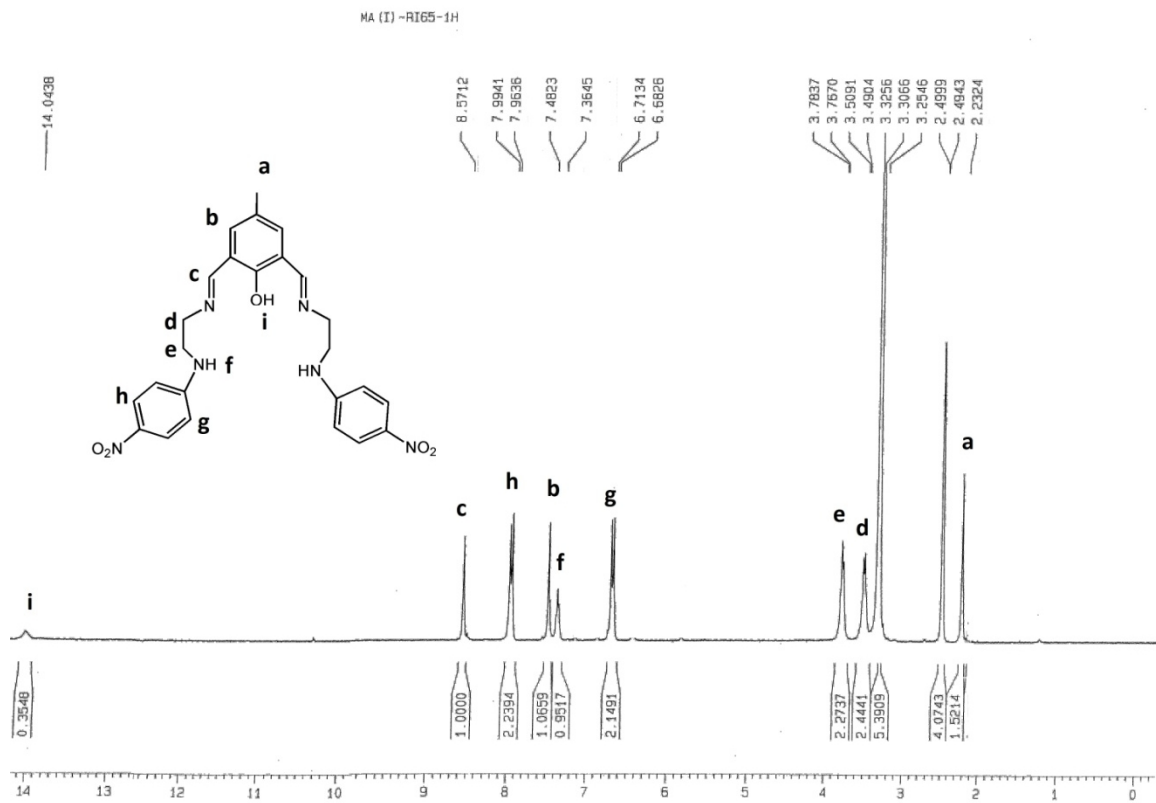


Fig. S1. ^1H NMR spectrum of DFC-EN-*p*-Ph-NO₂ in DMSO-d₆, in Bruker 300 MHz instrument.

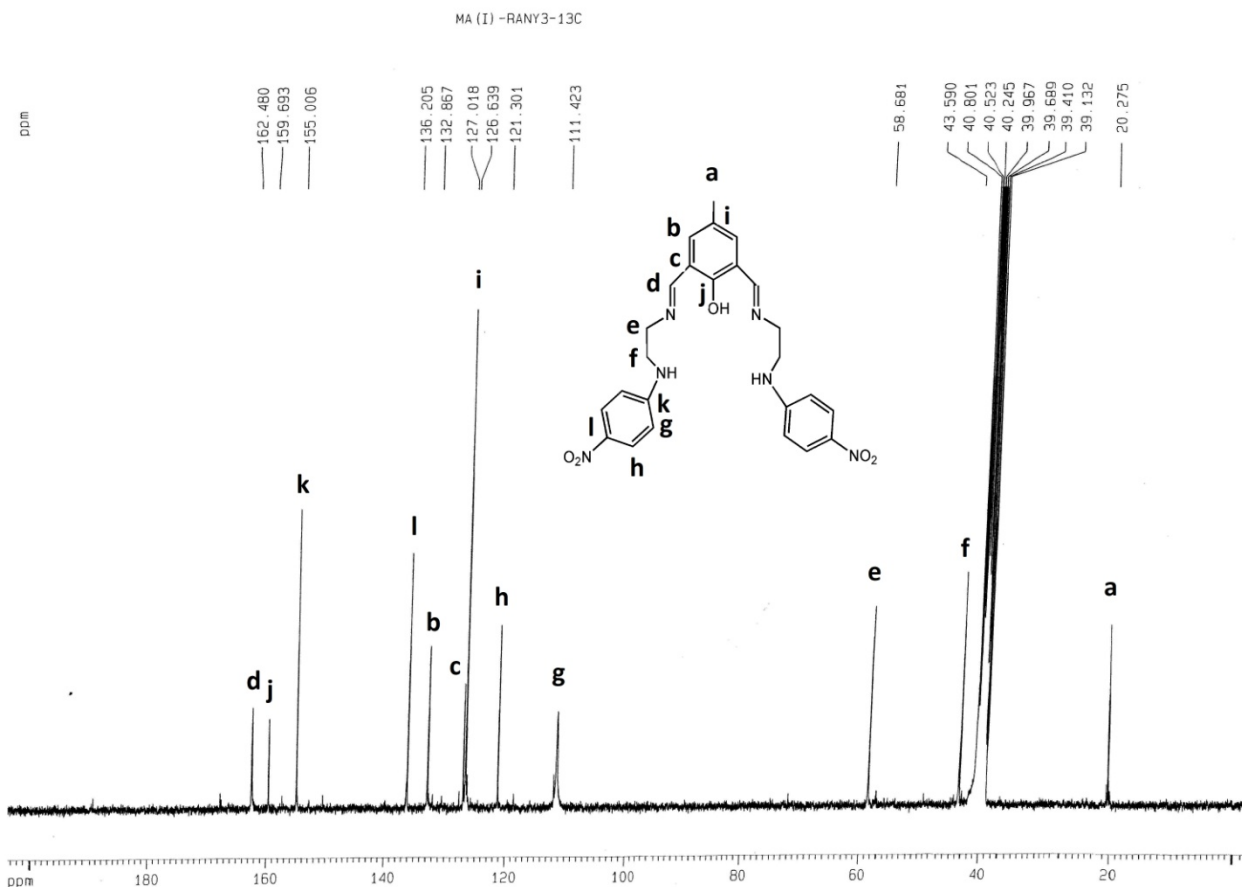


Fig. S2. ^{13}C NMR spectrum of DFC-EN-*p*-Ph-NO₂ in DMSO-d₆, in Bruker 300 MHz instrument

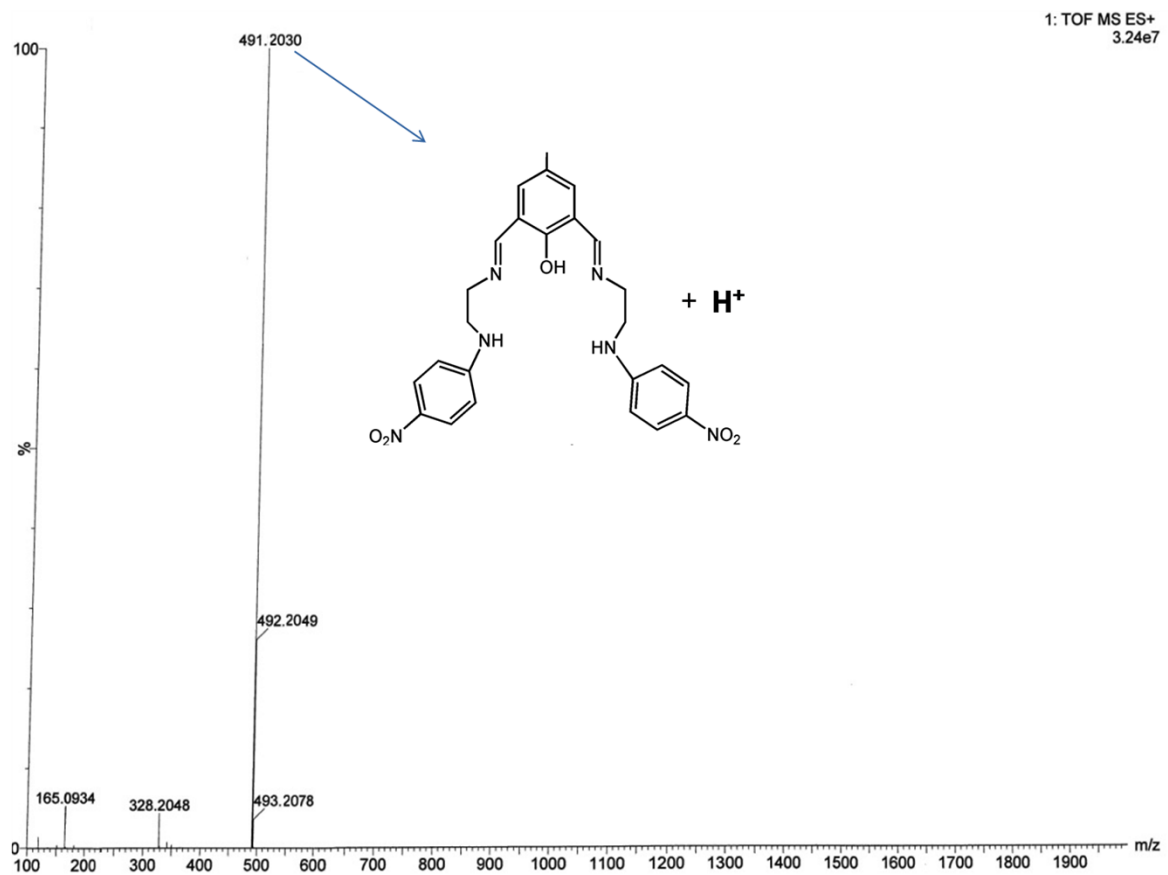


Fig.S3. Mass spectrum of DFC-EN-*p*-Ph-NO₂

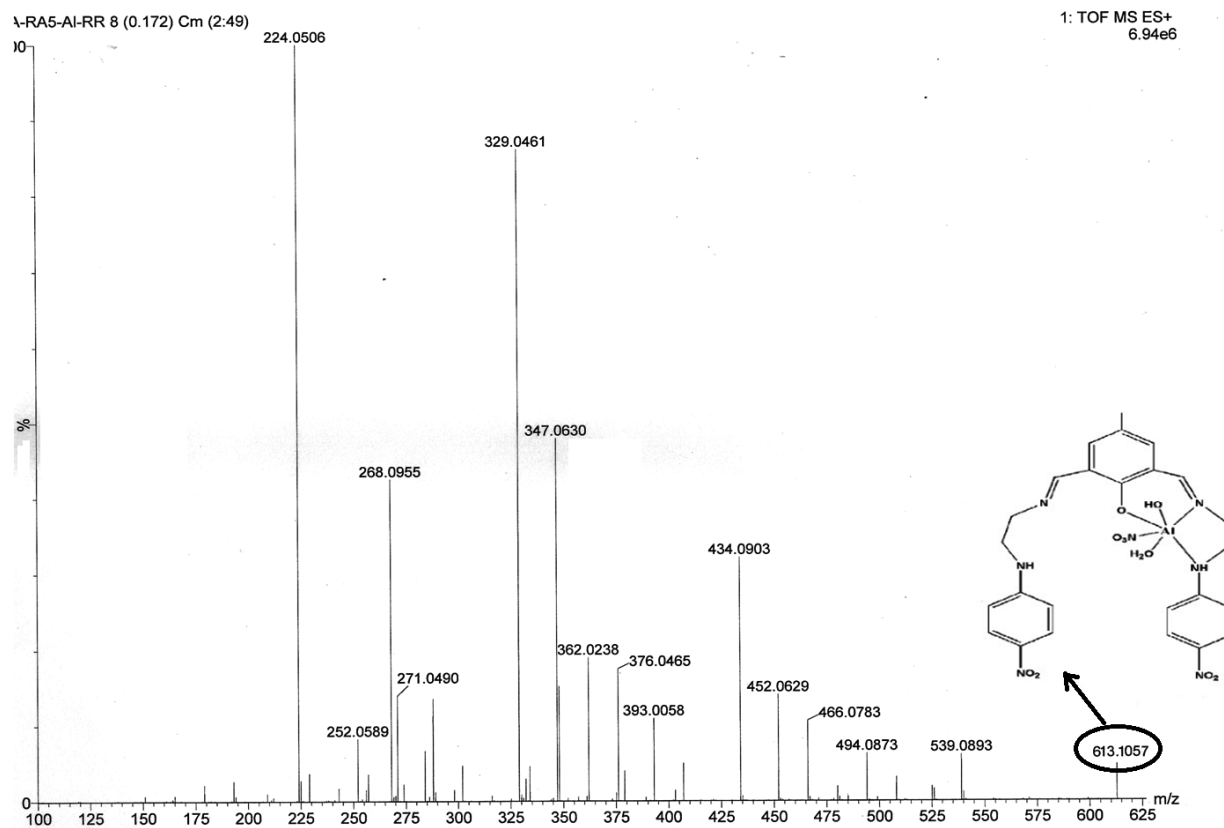


Fig.S3a. Mass spectrum of Al^{3+} complex below (m/z) 625 .

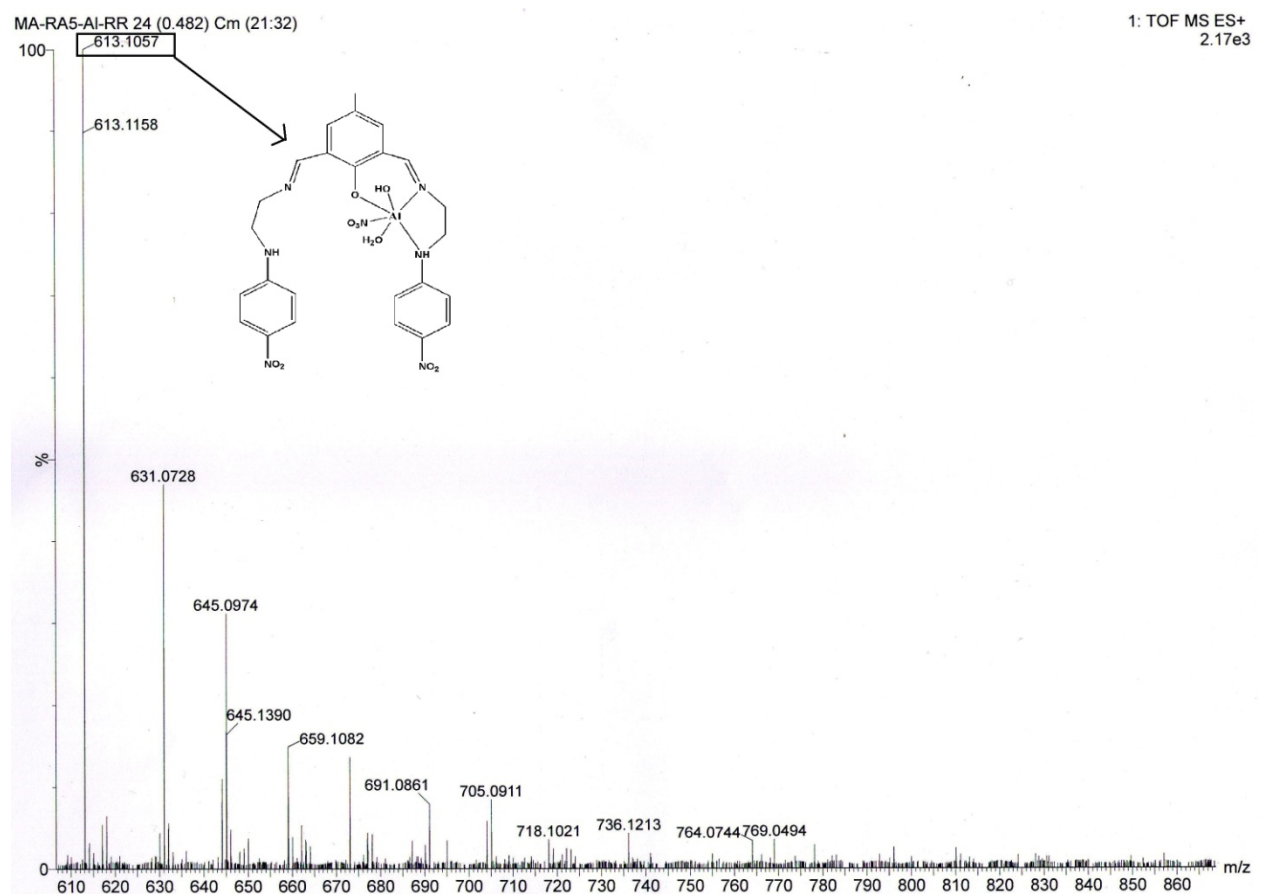


Fig.S3b. Mass spectrum of Al³⁺ complex.

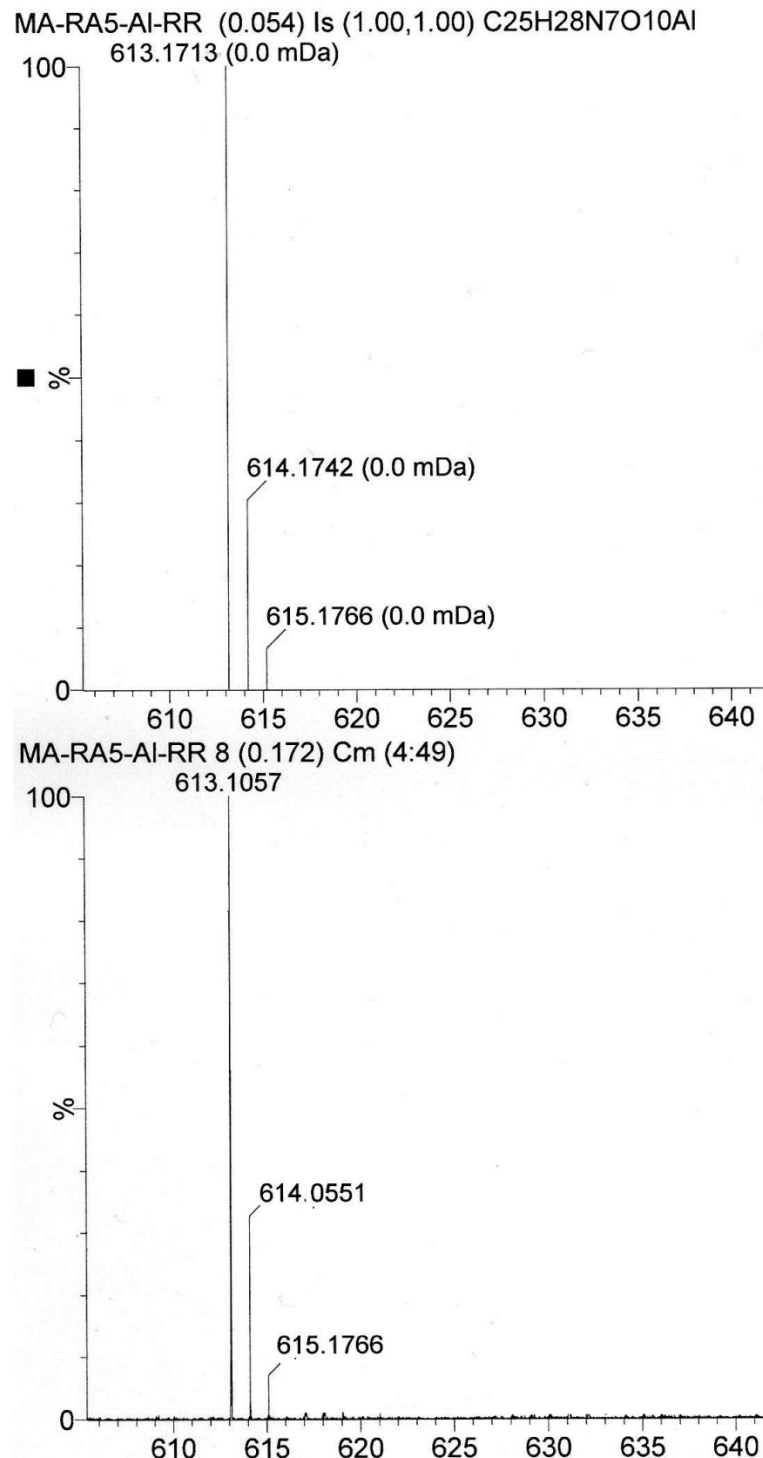


Fig.S3c. Simulated Mass spectrum of Al³⁺ complex.

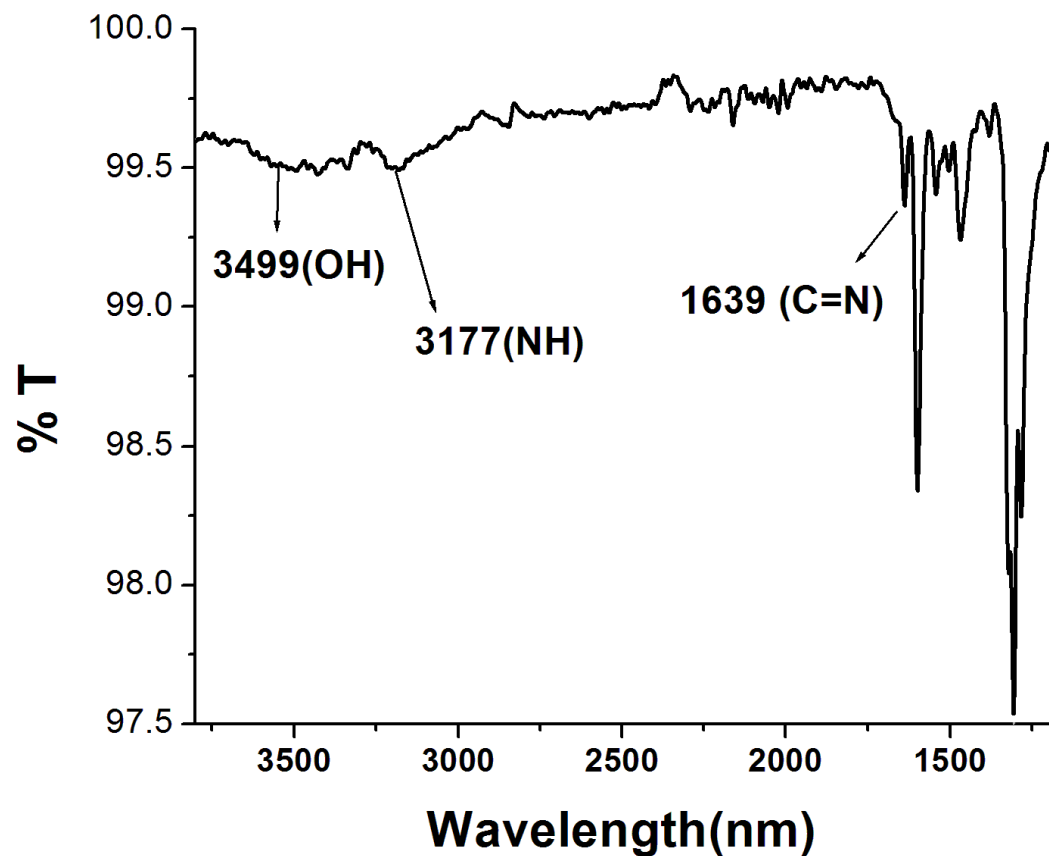


Fig. S4 .FT-IR spectrum of DFC-EN-*p*-Ph-NO₂ in MeOH .

JOB's Plot

This method is based on the measurement of a series of solutions in which molar concentrations of two reactants vary but their sum remains constant. The absorbance of each solution is measured at a suitable wavelength and plotted versus the mole fraction of one reactant. A maximum in fluorescence intensity occurs at the mole ratio corresponding to the combining ratio of the reactants. The composition of the complex was determined by JOB's method and found to be (1 : 1) with respect to ligand for Al^{3+} .

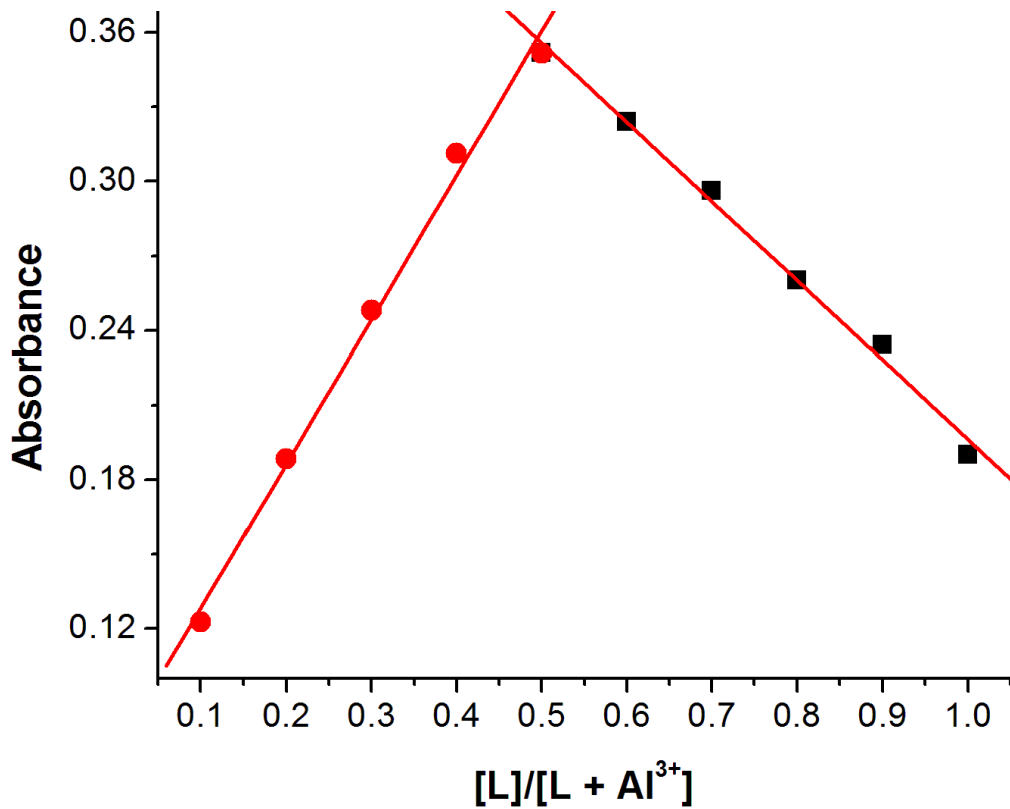


Fig.S5. Job's plot DFC-EN-*p*-Ph- NO_2 + Al^{3+}

Calculation for LOD value :

To determine the detection limit, fluorescence titration of **DFC-EN-p-Ph-NO₂** with Al³⁺ and PPi was carried out by adding aliquots of micromolar concentration of Al³⁺ and PPi.

However, The detection limit (LOD) of **DFC-EN-p-Ph-NO₂-Al³⁺** and **DFC-EN-p-Ph-NO₂-PPi** are calculated by 3σ method.

$$\text{LOD} = \frac{3 \times S_d}{\text{Slope}}$$

Where S_d is the standard deviation of blank, and Slope is from the plot of emission intensities versus Al³⁺ and PPi respectively.

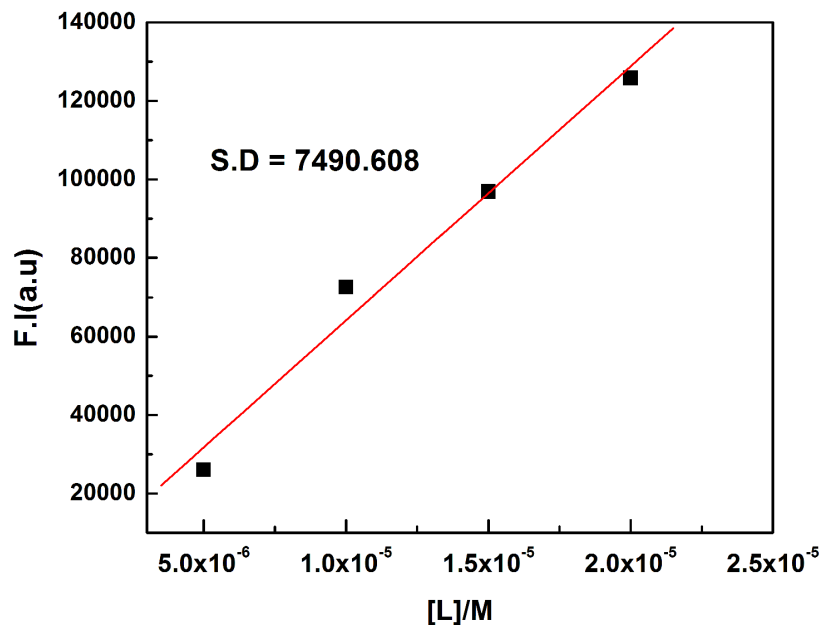


Fig.S6. Determination of S.D. of the blank, **DFC-EN-p-Ph-NO₂** solution.

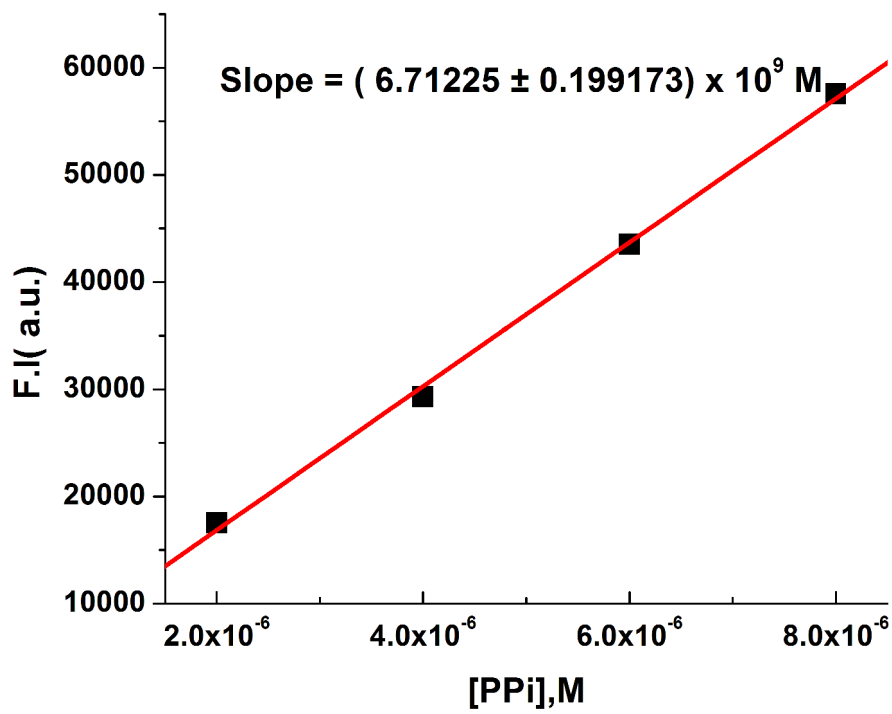


Fig.S6a. Linear dynamic plot of FI (at 534 nm) vs.[PPi] for the determination of S(slope);[DFC-EN-*p*-Ph-NO₂]=20μM

$$\text{LOD(PPi)}= (3 \times 7490.608) / 6.71225 \times 10^9$$

$$=3.34\mu\text{M}$$

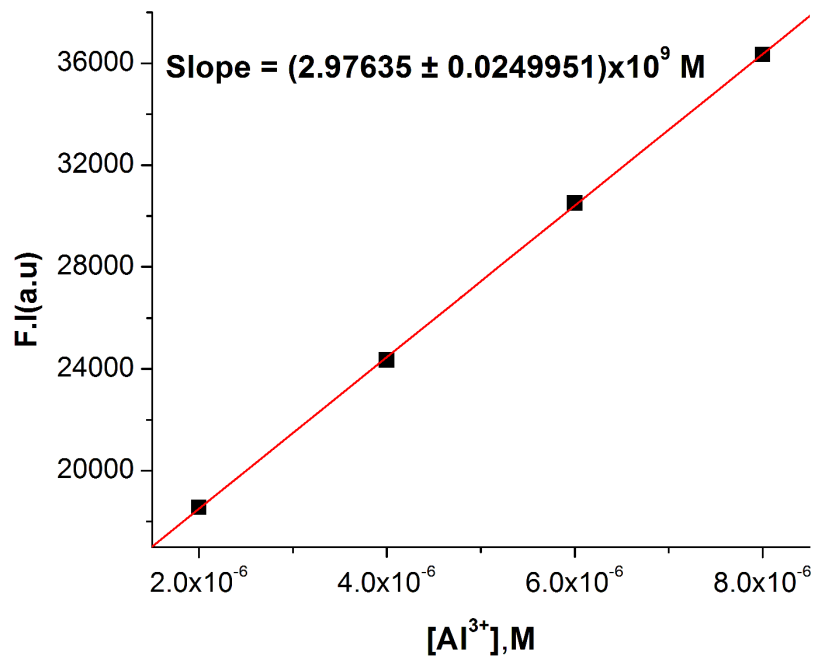


Fig.S6b. Linear dynamic plot of F.I. (at 486 nm) vs. [Al³⁺] for the determination of S(slope); [DFC-EN-*p*-Ph-NO₂]=20μM.

$$\text{LOD(Al}^{3+}\text{)} = (3 \times 7490.608) / 2.97635 \times 10^9$$

$$= 7.55 \mu\text{M}$$

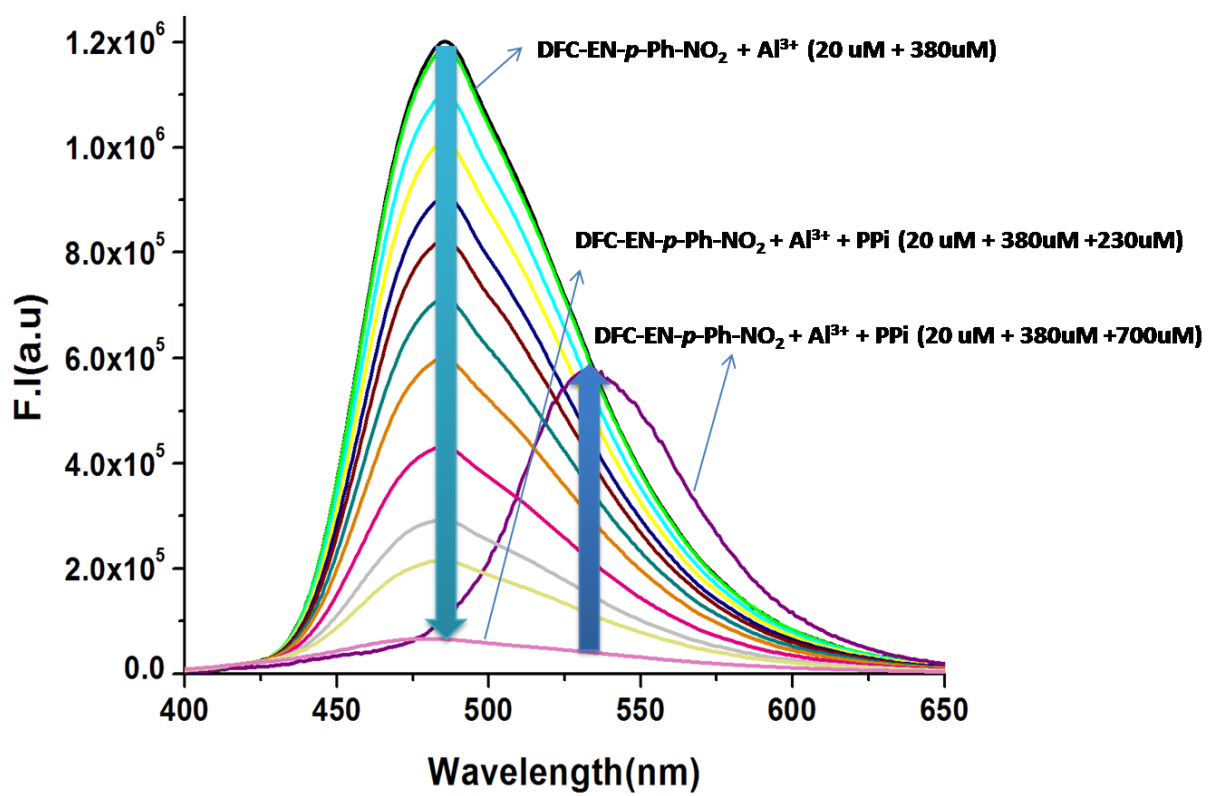


Fig.S7. Overall Spectra upon the addition of PPi on the Al³⁺ complex and in excess.

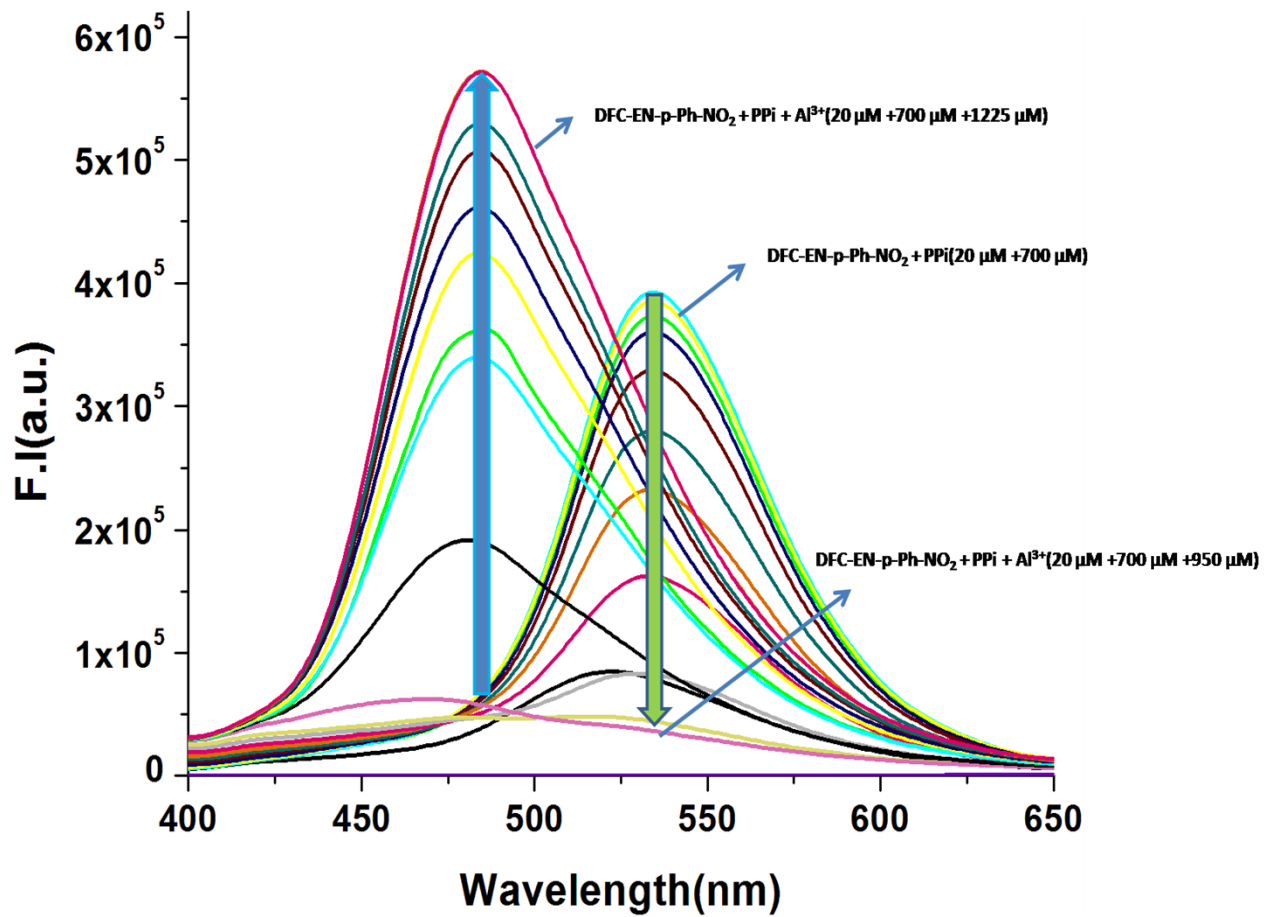


Fig.S8. Overall Spectra upon the addition of Al³⁺ on the PPi complex.

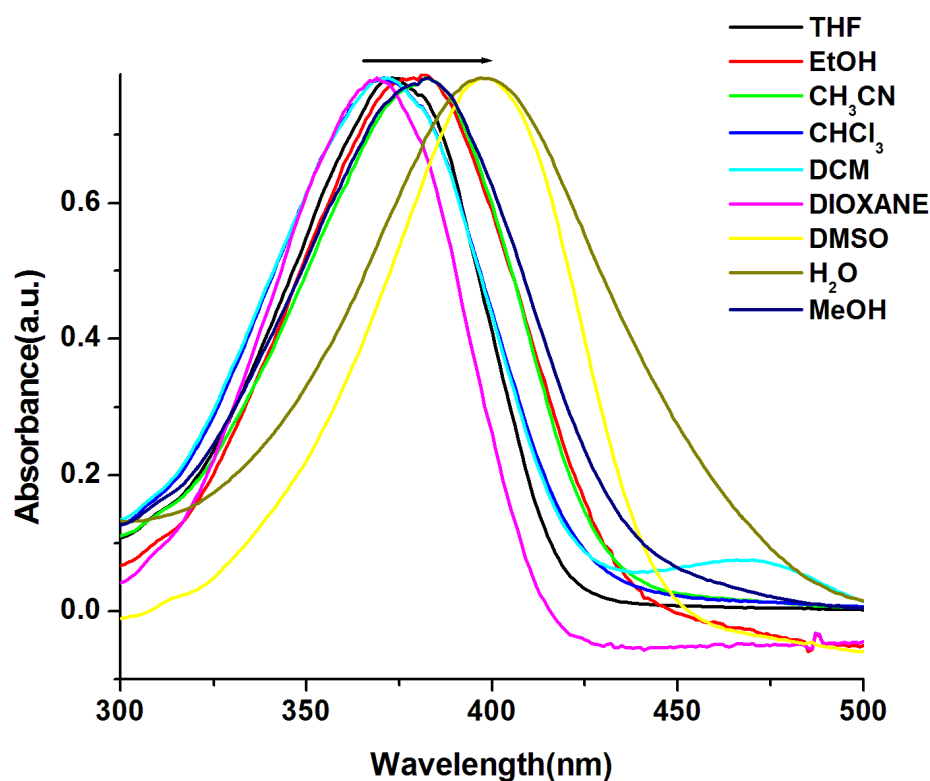


Fig.S9. Polarity dependence red shift of λ_{abs} of the Ligand (non-polar to polar)

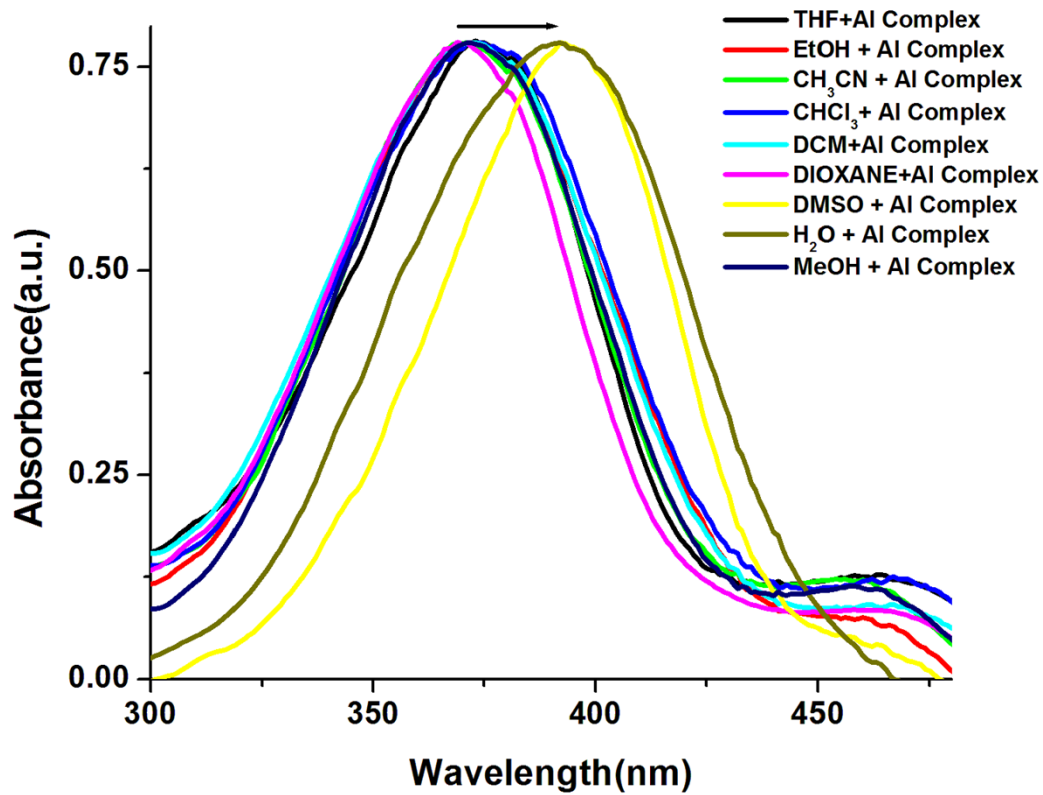


Fig.S9a. Polarity dependence red shift of λ_{abs} of the Al- complex (non-polar to polar)

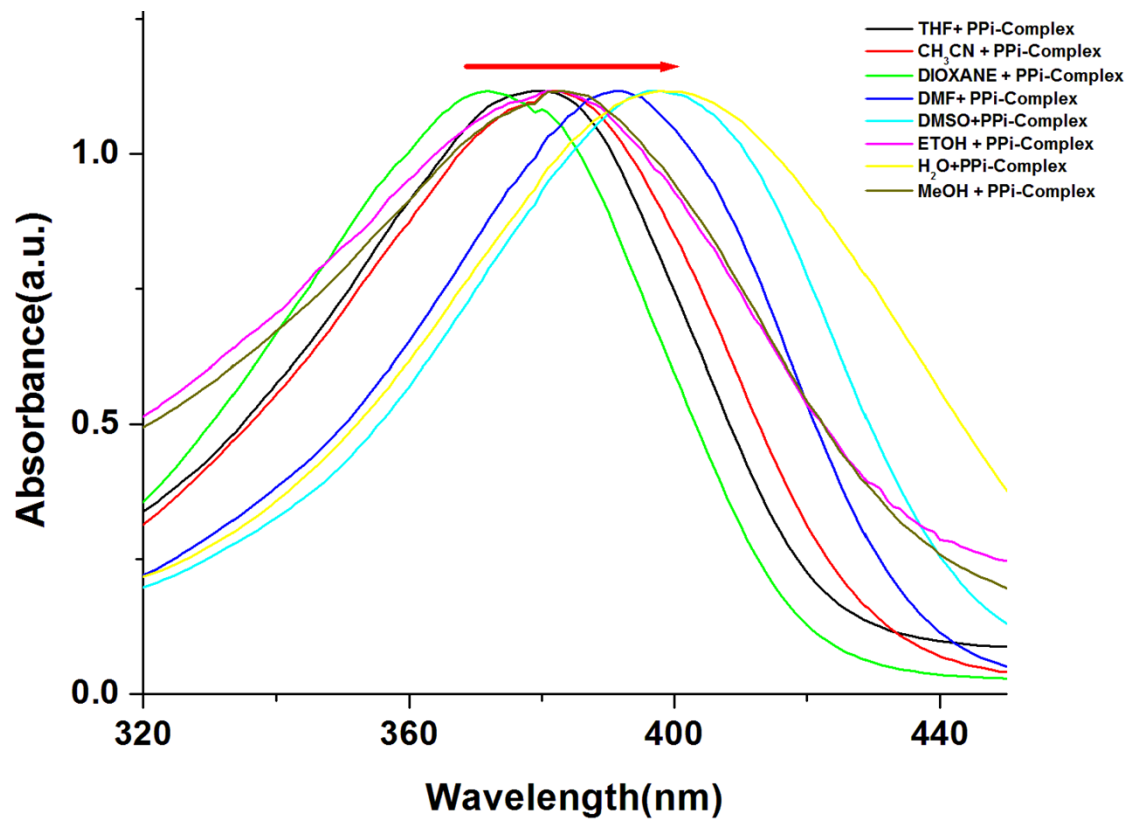


Fig.S9b. Polarity dependence red shift of λ_{abs} of the ligand-PPi complex (non-polar to polar).

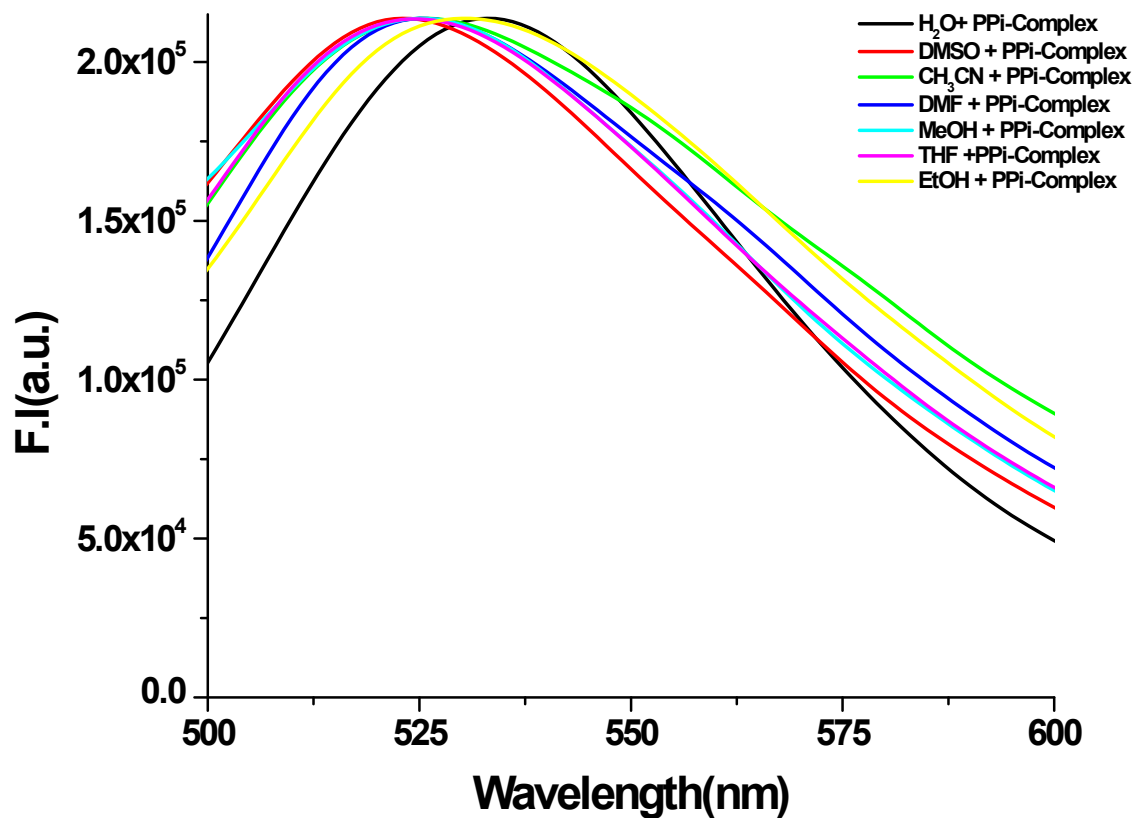


Fig.S9c. Polarity dependence shift of λ_{em} of the ligand-PPi complex. (non-polar to polar)

Quantum Yield Determination:

Fluorescence quantum yields (Φ) were estimated by integrating the area under the fluorescence

$$\text{curves with the equation: } \Phi_{sample} = \frac{OD_{std}}{OD_{sample}} \times \frac{A_{sample}}{A_{std}} \times \Phi_{std}$$

where, A was the area under the fluorescence spectral curve, OD was optical density of the compound at the excitation wavelength and η was the refractive indices of the solvent. Quinine sulphate was used as quantum yield standard (quantum yield is 0.54 in water)for measuring the quantum yields of **DFC-EN-*p*-Ph-NO₂** and **[DFC-EN-*p*-Ph-NO₂ +Al³⁺]** and **[DFC-EN-*p*-Ph-NO₂ +PPi]** systems.

Table S1

DFC-EN-<i>p</i>-Ph-NO₂	14.04(i)	8.57 (c)	7.36 (f)
DFC-EN-<i>p</i>-Ph-NO₂ + PPi	-----	8.49 (c)	7.25 (f)
DFC-EN-<i>p</i>-Ph-NO₂+ Al³⁺	-----	9.42, 10.17 (c)	7.17 (f)

DFT calculations

DFT calculations on **DFC-EN-*p*-Ph-NO₂**, **DFC-EN-*p*-Ph-NO₂- Al³⁺** and **DFC-EN-*p*-Ph-NO₂- PPi** were fully optimized using Gaussian 09W software package.¹ The B3LYP functional has been adopted with 6-31G as basis set for all the atoms (Al, C, H, N and O) for both the ligand and its Al³⁺ complex. In case of **DFC-EN-*p*-Ph-NO₂-PPi** we used 6-31G+G(d,p) basis set. Gauss Sum 2.1 programme was used to calculate the molecular orbital contributions from groups or atoms.

Geometry optimization

The optimized geometry of **DFC-EN-*p*-Ph-NO₂** and its Al³⁺complex (**3**) are shown in **Fig. S9**.

Both **DFC-EN-*p*-Ph-NO₂** and its Al³⁺complex (**3**) have C1 point group. The free ligand is H-

bonded between phenolate –OH and azomethyne-N atom O–H···N = 1.63 Å, \angle O–H···N = 147.46°. In **DFC-EN-*p*-Ph-NO₂ – Al³⁺** the Al³⁺ center is in a distorted octahedral geometry surrounded by one azomethyne-N, one imine-N and phenoxy-O, one –O(NO₃⁻) in a square plane while one OH and one H₂O molecule occupy the axial positions. Selected bond distances and angles are listed in Table S2 and comparable to the literature values.^{2,3} In **DFC-EN-*p*-Ph-NO₂ – PPi** there are H-bonding between phenoxy-OH and O70 atom of PPi with O9–H62•••O70 = 1.70 Å, \angle O9–H62•••O70 = 130.16° ; and imine (NH) proton and =O65 of PPi with and N32-H34•••O65 = 1.41 Å, \angle N32-H34•••O65 = 176.5°. Selected bond distances and angles of **DFC-EN-*p*-Ph-NO₂ – PPi** complex are listed in **Table S3**.

Table S2a: Selective bond distance and bond angles of DFC-EN-*p*-Ph-NO₂ + Al³⁺ complex.

Bond distance(Å)		Bond angles(°)	
Al61-O63	2.089	O9 Al61 O67	108.87
O9-Al61	1.853	O9 Al61 O62	101.97
N33-Al61	2.249	O9 Al61 O63	78.83
C20-N18	1.477	O9 Al61 N33	158.71
N18-Al61	2.017	N33 Al61 O67	90.25

O62-Al61	1.917	N18 Al61 O9	88.42
Al61-O67	1.780		

Table S2b: Selective bond distance and bond angles of DFC-EN-*p*-Ph-NO₂.

Bond distance(Å)		Bond angles(°)	
C15-N19	1.299	C2 O13 H14	108.36
O13-H14	1.026	C16 N20 C22	124.04
C16-N20	1.284	C2 O13 H14	108.36
C2-O13	1.363	C3 C15 N19	122.14
N35-C47	1.380	C28 N33 H34	113.13
C28-H33	1.456	C28 N33 C37	126.00

Table S3: Selective bond distance and bond angles of DFC-EN-*p*-Ph-NO₂ + PPi complex.

Bond distance(Å)		Bond angles(°)	
C2-O9	1.39	O65 P63 O75	110.79
P64-O70	1.60	O66 P63 O75	102.71
N32-H34	1.007	O68 P64 O70	117.98
P63-O65	1.578	O68 P64 O75	98.54
C27-N32	1.465	O65 P63 O75	110.79

		O66 P63 O75	102.71
--	--	-------------	--------

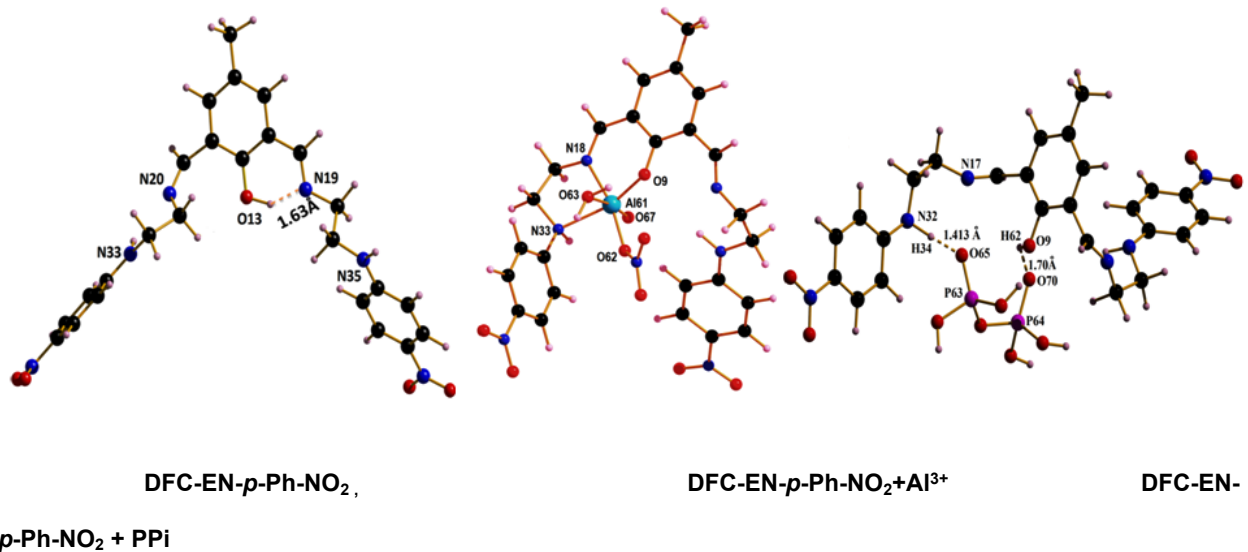


Fig.S10. DFT/B₃LYP optimized geometry of ligand DFC-EN-*p*-Ph-NO₂ as well as complexes with Al³⁺ and PPi.

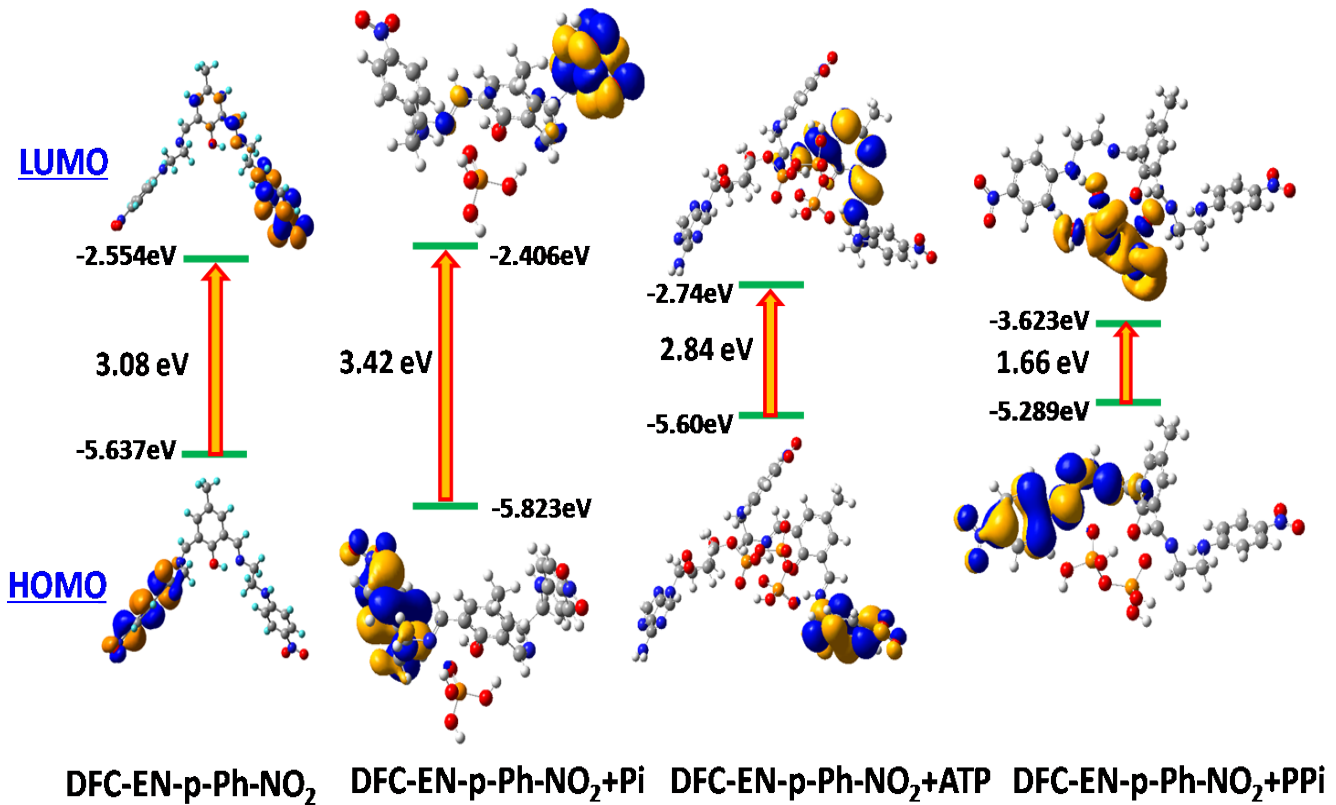


Fig.S11. HOMO-LUMO energy separation in ligand DFC-EN-p-Ph-NO₂ as well as complexes with Pi, ATP and PPi.

Table S4: The comparable calculated optical transitions with Experimental UV/Vis values for the ligand (DFC-EN-*p*-Ph-NO₂) and complex (3)

Ligand and Complex(3)	Theoretical (nm)	Experimental (nm)	Electronic Transition	f
Ligand	387.93	388	S ₀ →S ₃	0.0185
Ligand	384.95		S ₀ →S ₄	0.6123
Complex(3)	370.43	371	S ₀ →S ₆	0.0649
Complex(3)	367.09		S ₀ →S ₇	0.0118

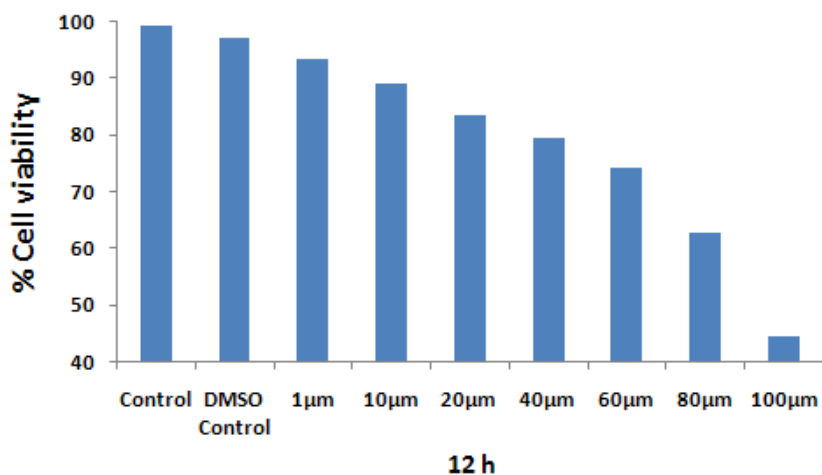


Fig.S12. MTT assay.

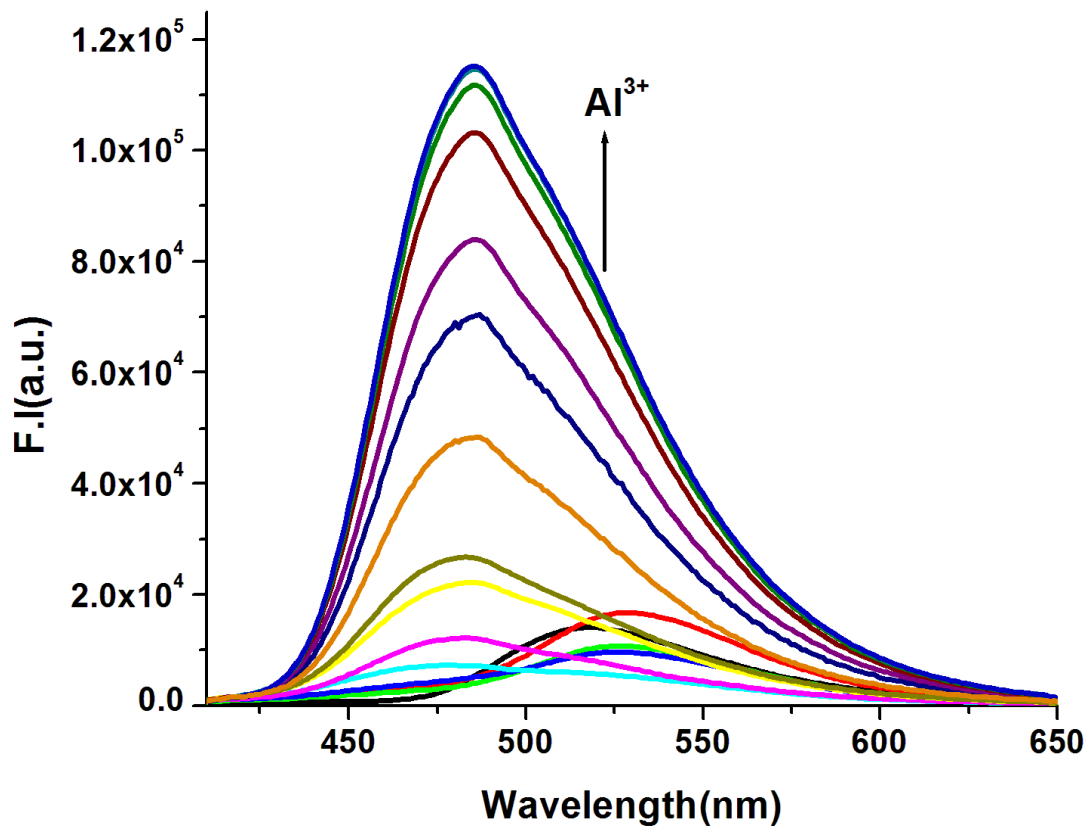


Fig. S13. Fluorescence titration of 2 μ M **DFC-EN-p-Ph-NO₂** in MeOH-H₂O (8:2, v/v) in HEPES buffer at pH 7.2 by the gradual addition Al³⁺ with $\lambda_{\text{ex}} = 370$ nm, $\lambda_{\text{em}} = 486$ nm.

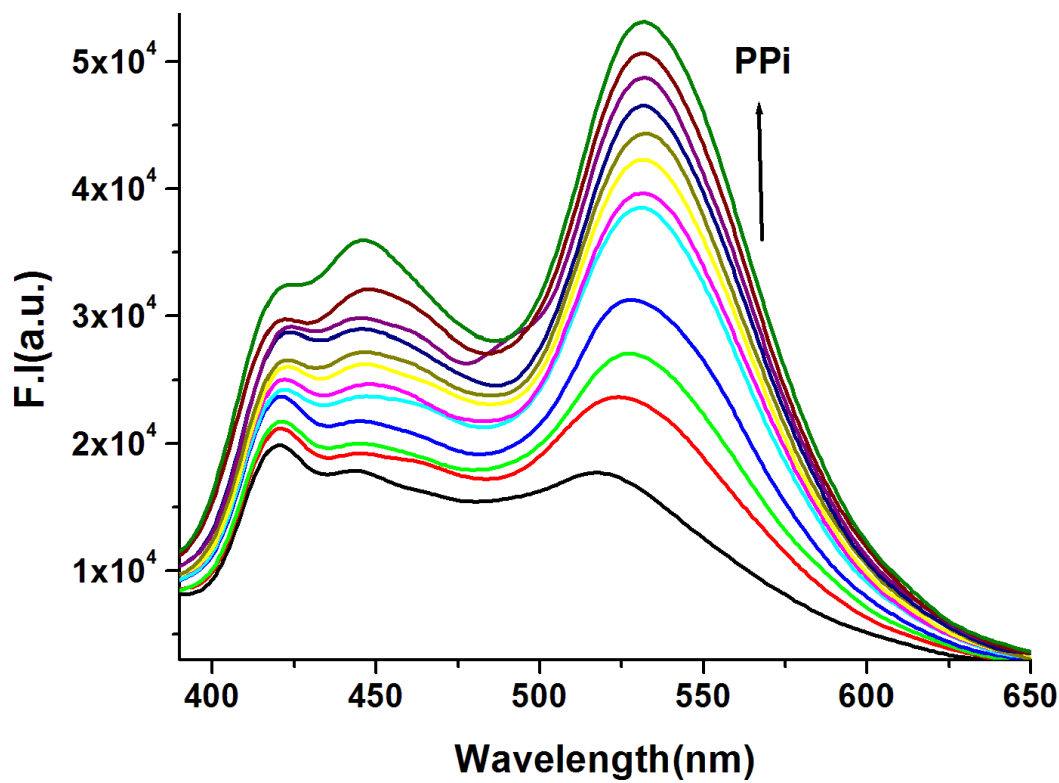


Fig. S14. Fluorescence titration of 2 μ M DFC-EN-*p*-Ph-NO₂ in MeOH-H₂O (8:2, v/v) in HEPES buffer at pH 7.2 by the gradual addition PPi with $\lambda_{\text{ex}} = 370$ nm, $\lambda_{\text{em}} = 534$ nm.

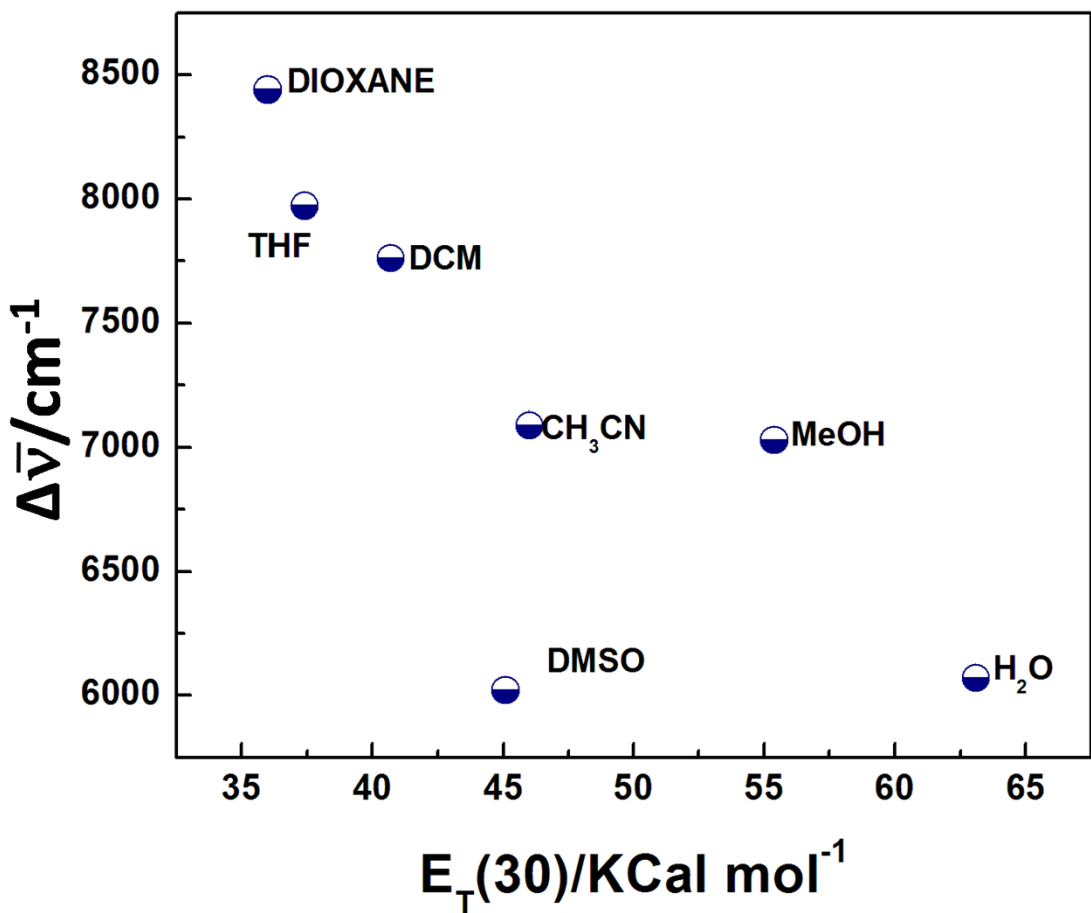


Fig. S15. Plot of Stokes shift ($\Delta\bar{v}$) vs solvent polarity parameter $E_T(30)$ in different solvents.

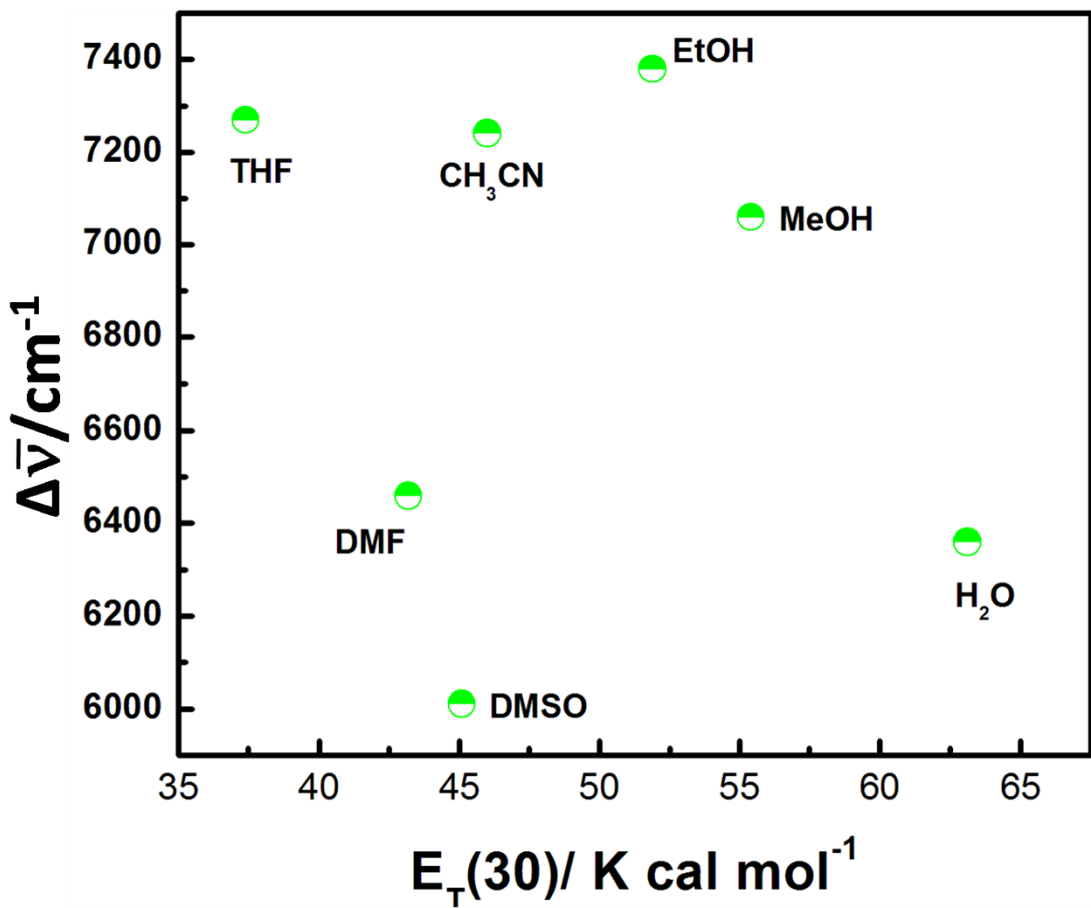


Fig. S16. Plot of Stokes shift ($\Delta\bar{v}$) vs solvent polarity parameter $E_T(30)$ in different solvents.

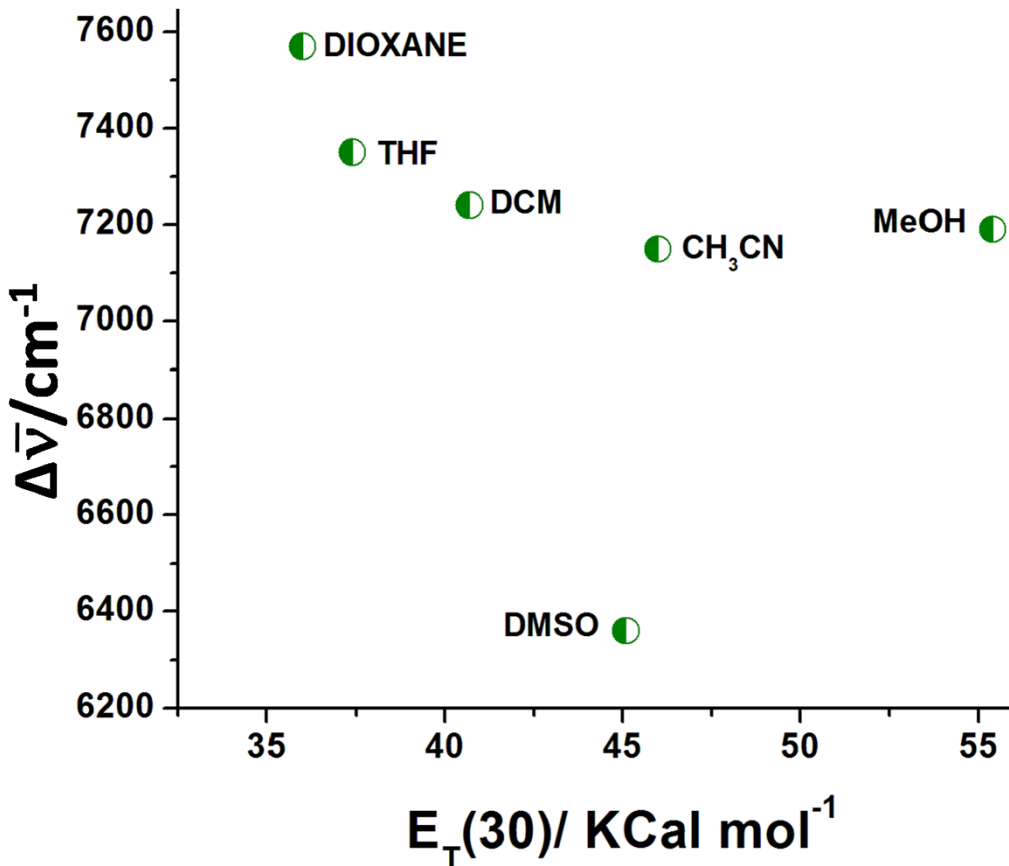


Fig. S17. Plot of Stokes shift (Δv) vs solvent polarity parameter $E_T(30)$ in different solvents.

1. M. J. Frisch, G. W. Trucks, H. B. Schlegel, G. E. Scuseria, M. A. Robb, J. R. Cheeseman, G. Scalmani, V. Barone, B. Mennucci, G. A. Petersson, H. Nakatsuji, M. Caricato, X. Li, H. P. Hratchian, A. F. Izmaylov, J. Bloino, G. Zheng, J. L. Sonnenberg, M. Hada, M. Ehara, K. Toyota, R. Fukuda, J. Hasegawa, M. Ishida, T. Nakajima, Y. Honda, O. Kitao, H. Nakai, T. Vreven, J. A. Montgomery Jr., J. E. Peralta, F. Ogliaro, M. Bearpark, J. J. Heyd, E. Brothers, K. N. Kudin, V. N. Staroverov, R. Kobayashi, J. Normand, K. Raghavachari, A. Rendell, J. C. Burant, S. S. Iyengar, J. Tomasi, M. Cossi, N. Rega, J. M. Millam, M. Klene, J. E. Knox, J. B. Cross, V. Bakken, C. Adamo, J. Jaramillo, R. Gomperts, R. E. Stratmann, O. Yazyev, A. J. Austin, R. Cammi, C. Pomelli, J. W. Ochterski, R. L. Martin, K. Morokuma, V. G. Zakrzewski, G. A. Voth, P. Salvador, J. J. Dannenberg, S. Dapprich, A.

- D. Daniels, Ö. Farkas, J. B. Foresman, J. V. Ortiz, J. Cioslowski and D. J. Fox, Gaussian 09, (Revision A.1), Gaussian, Inc., Wallingford, CT, 2009.
2. R. Bhowmick, M. Dolai, R. Alam, T. Mistri, A. Katarkar, K. Chaudhuri and M. Ali, *RSC Adv.*, 2014, **4**, 41784.
 3. G. Sivaraman, T. Anand and D. Chellappa, *RSC Adv.*, 2012, **2**, 10605.